SOFIA-EXES Observations of Betelgeuse during the Great Dimming of 2019/2020

Graham M. Harper[1] , Curtis N. DeWitt[2] , Matthew J. Richter[3] , Edward F. Guinan[4] , Richard Wasatonic[4], Nils Ryde[5] ,
Edward J. Montiel[2], and Amanda J. Townsend[3]

[1] Center for Astrophysics and Space Astronomy, University of Colorado Boulder, 389 UCB, Boulder, CO 80309, USA; graham.harper@colorado.edu
[2] USRA/SOFIA, NASA Ames Research Center, Moffett Field, CA 94-35, USA
[3] Department of Physics, University of California Davis, Davis, CA 95616, USA
[4] Astrophysics and Planetary Science Department, Villanova University, Villanova, PA 19085, USA
[5] Department of Astronomy and Theoretical Physics, Lund University, Lund, Sweden
Received 2020 March 18; revised 2020 March 26; accepted 2020 March 30; published 2020 April 14

Abstract

In 2019 October Betelgeuse began a decline in *V*-band brightness that went beyond the minimum expected from its quasi-periodic $\sim$420 day cycle, becoming the faintest in recorded photometric history. Observations obtained in 2019 December with Very Large Telescope/SPHERE have shown that the southern half of the star has become markedly fainter than in 2019 January, indicating that a major change has occurred in, or near, the photosphere. We present Stratospheric Observatory for Infrared Astronomy (SOFIA) Echelon Cross Echelle Spectrograph (EXES) high spectral-resolution observations of [Fe II] 25.99 μm and [S I] 25.25 μm emission lines from Betelgeuse obtained during the unprecedented 2020 February *V*-band brightness minimum to investigate potential changes in the circumstellar flow. These spectra are compared to observations obtained in 2015 and 2017 when the *V* magnitude was typical of brighter phases. We find only very small changes in the gas velocities reflected by either of the line profiles, no significant changes in the flux to continuum ratios, and hence no significant changes in the [Fe II]/[S I] flux ratios. There is evidence that absorption features have appeared in the 2020 continuum. The Alfvén wave-crossing time from the upper photosphere is sufficiently long that one would not expect a change in the large-scale magnetic field to reach the circumstellar [Fe II] and [S I] line-forming regions, $3 < R\ (R_*) < 20$. However, the light-crossing time is of order a few hours and a reduction in luminosity may reduce the dust-gas heating rate and [O I] 63.19 μm emission, which has contributions from $R > 20R_*$, where significant circumstellar oxygen-rich dust is observed.

1. Introduction

Betelgeuse (α Orionis, HD 39801, HR 2061) is a massive nearby red supergiant (RSG) that is destined to undergo core-collapse to become either a supernova or implode directly into a black hole. RSGs and supernovae play an important role in the chemical evolution and shaping of galaxies but, despite this, the RSG phase of evolution is not well understood. This is, in part, because the stellar evolution depends on both mass loss and rotation, which are not well characterized (e.g., Meynet et al. 2015). Furthermore, there is no *standard model* that can predict mass-loss rates from RSGs and which can explain the panoply of observed stellar outflow diagnostics. This problem is particularly acute for K and early M supergiants, including well-known stars such as Betelgeuse and Antares, because their outflows are under-abundant in molecules and dust compared to their later-spectral-type counterparts, where radiation pressure on molecules and/or dust may drive outflows.

Betelgeuse's large angular size and brightness have resulted in it being extensively studied at multiple wavelengths over the last century, with some recent studies presented in Kervella et al. (2013). These studies seek to unravel the puzzling origins of different species of dust seen at different radii, the extended photosphere and chromosphere, quasi-steady outflows, photospheric hot spots, and atmospheric asymmetries.

Early photometric (Stebbins 1931) and radial velocity studies (Spencer Jones 1928; Sanford 1933) both revealed a period of $\simeq$5.8 yr ($\simeq$2100 day) with peak-to-peak variations of 0.44 mag, and $\simeq$4–6 km s^{-1}, respectively. A discussion of

these data and observations over the next few decades is given by Goldberg (1984). In addition to shorter ($\sim$ week) timescale fluctuations, the early photometric data also showed indications of a $\sim$420 day period later discovered in the satellite ultraviolet and *B* magnitude data by Dupree et al. (1987), and confirmed in the radial velocity study of Smith et al. (1989). Betelgeuse has an MK spectral-type of M1-M2 Ia-ab (Keenan & McNeil 1989), but it also exhibits a variable spectral-type; White & Wing (1978) used narrow-band photometric TiO and CN indices to derive a mean spectral-type of M2.2 with a range of M1.5–M2.7 between 1969 and 1976. Despite the lack of a clear constant phase relation between the radial velocity and light curve data, the variations probably result from the interaction of convection in the outer envelope and pulsation (Kiss et al. 2006). How these photospheric variations are connected to the heating of the extended atmosphere and circumstellar envelope (CSE), and the ejection of mass is not known. It is of particular interest given the importance of RSGs as SN II progenitors, e.g., Betelgeuse, with an initial mass of $\sim$20 $M_\odot$ (Harper et al. 2008; Dolan et al. 2016), continuing its currently mass-loss rate might eventually undergo core-collapse to become either a SN II-P (Smith et al. 2009) or implode directly into a black hole (Smartt 2009; Sukhbold & Adams 2020). While parts of the chromosphere show evidence of non-radial motions (Lobel & Dupree 2001), the circumstellar outflow velocities appear dynamically decoupled from the photospheric radial velocity variations (Weymann 1962).

The CSE consists of a dominant gas phase of neutral and singly ionized atomic species, together with under-associated CO and oxygen-rich dust. For Betelgeuse, beyond the extended chromosphere at $\simeq 1.75\,R_*$ (O'Gorman et al. 2015), there are two well-determined outflows, an inner flow of $\simeq 9\,\mathrm{km\,s^{-1}}$ that extends out to $\sim 4''$, and an outer flow of $16\,\mathrm{km\,s^{-1}}$ that extends beyond $32''$ (O'Gorman et al. 2012, and references therein). 7.76–19.50 μm imaging with Very Large Telescope (VLT)/ VISIR reveals dust emission from an irregular ring-like structure between $0''5$ and $1''0$ (23–45 R_*, assuming a photospheric angular diameter of $\phi = 44$ mas) from the star, and more diffuse irregular emission out to $3''$ (Kervella et al. 2011, and references therein). Three bright plumes also appear to extend in toward the star and two of these correspond to near-photospheric features seen in VLT/NACO JHK images (Kervella et al. 2009). Closer to the star, dust has also been detected in a shell near $3R_*$ in VLT/SPHERE/ZIMPOL polarization images (Kervella et al. 2016). How the gas and dust are mixed is not known, but where they co-exist dust grains will be driven by the stellar radiation field and heat the gas through collisions.

The dynamical timescale for motions, shocks, or magnetic waves to reach the circumstellar outflow are of the order of years to decades, but Haas et al. (1995) observed that [O I] 63.19 μm emission fluxes, formed between 3 and 100 R_*, might be responsive to changes in the photospheric V magnitude. They noted that two observations made with the Cryogenic Grating Spectrometer on the Kuiper Airborne Observatory (KAO) taken 22 months apart, on 1992 January 16 ($F = 2.4 \pm 0.2\,\mathrm{W\,cm^{-2}}$, $V \sim 0.35$; Haas & Glassgold 1993) and 1993 November ($F = 1.1 \pm 0.2\,\mathrm{W\,cm^{-2}}$, $V \sim 0.59$), showed a factor of two decrease in flux when the V magnitude increased by 0.24, and an observation with the Far-Infrared Imaging Fabry–Perot Interferometer (FIFI) on KAO in 1993 March gave a non-detection with an upper-limit of $F(3\sigma) < 0.6\,\mathrm{W\,cm^{-2}}$ ($V \sim 0.88$) when the V magnitude was 0.29 mag higher again. More recently Castro-Carrizo et al. (2001) reported a 1997 September 12 ISO LWS02 flux of $F = 1.93 \pm 0.06\,\mathrm{W\,cm^{-2}}$ when $V \sim 0.57$. The V magnitudes near the times of these observations are from Krisciunas (1992, 1994) and Figure 1. If there is a causal connection between V magnitudes and [O I] 63.19 μm flux, then it must be related to changes in the radiation interacting with dust in the gaseous outflow where the flux is emitted, and which can occur on timescales of a few hours. For dust-gas heating the [O I] 63.19 μm fluxes related to changes in stellar luminosity before the observations were obtained. We also note that Skinner et al. (1997) reported a decrease in the surface brightness of UKIRT 9.7 and 12.5 μm CSE silicate images, extending out to $3''$–$4''$, over a 1 yr interval during the time when there was a sudden decrease in V-band brightness (Guinan et al. 1993).

Since 2019 October Betelgeuse has undergone a deep decline of over 1.1 mag (Guinan et al. 2020), exceeding the previous quasi-periodic minimum of $V \simeq 0.9$ mag, and becoming the faintest it has been in modern record at $V = 1.61$ mag during 2020 February 7–13. Figure 1 shows V photometry obtained over a span of the last 23 yr obtained at the Wasatonic Observatory, Villanova University where it can be seen that while the most recent minimum has occurred close in time to that expected based on previous cycles, its depth is unprecedented. Observations obtained in 2019 December with the
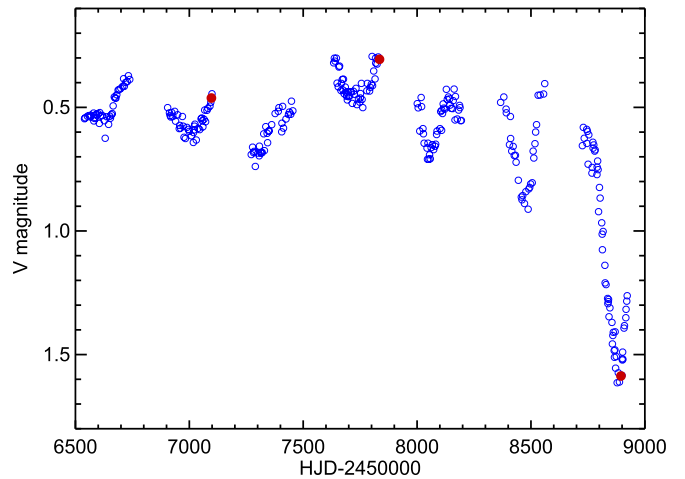
Figure 1. V magnitude photometry of Betelgeuse (blue circles) obtained at the Wasatonic Observatory, Villanova University. These data clearly show the quasi-periodic ~ 420 day variations, and periodogram analyses reveal the longer 5.8 yr period. The amplitudes and periods all appear to change. Also shown are the magnitudes at the 2015, 2017, and 2020 epochs of the Echelon Cross Echelle Spectrograph (EXES) observations (red-filled). It can be seen that the Cycle 2 (2015) and Cycle 5 (2017) spectra were obtained in brighter phases, while the Cycle 7 DDT observations were made at the minimum of the 2019/2020 dimming.

VLT/SPHERE in the CntHa filter ($\lambda 644.9$, $\Delta\lambda = 4.1$ nm; M. Montargès 2020,[6] private communication) have shown that the southern half of the photosphere has become markedly fainter than in 2019 January. Potential causes for the deep decline beyond the typical minimum are a continued cooling of the photosphere leading to deep TiO absorption bands in the V-band and/or the formation of dust obscuring the photosphere. Levesque & Massey (2020) find that the mean T_{eff} has declined slightly, but this is not sufficient to explain the optical dimming, and they propose that the presence of new large-grain dust in the line of sight is a possible explanation for the recent photometric changes.

Betelgeuse is currently being observed as part of an ongoing 2019/2020 CfA MOB program and with the continued decline of the V brightness reported by Guinan & Wasatonic (2020) astronomers have been actively studying the response of Betelgeuse with multi-wavelength observatories. Based on community inputs of the potential scientific importance of the Betelgeuse event, the Director of Science Mission Operations for NASA-DLR's Stratospheric Observatory for Infrared Astronomy (SOFIA) initiated a set of DDT observations of the star in winter/spring 2020. These observations have, or will, cover all the instruments scheduled to fly on the airplane in the period in question (Echelon Cross Echelle Spectrograph (EXES), FIFI-LS, upGREAT, and FORCAST).

Here we present SOFIA-EXES [Fe II] 25.99 μm and [S I] 25.25 μm emission line spectra that form part of this campaign as a concerted effort to gain empirical constraints on the unprecedented dimming of Betelgeuse. These diagnostics are described in Table 1. The EXES observations presented here provide an examination of the line-forming region, $2 < R_*\ (R_\odot) < 20$ between the photosphere and overlapping the [O I] 63.19 μm forming region, $2 < R_*\ (R_\odot) < 130$ (Harper et al. 2009).

Table 1
EXES Forbidden Line Diagnostic Transitions

Species	Transition Upper → Low	Wavenumber (cm^{-1})	Wavelength (μm)	E_{up} (K)	Einstein A-value (s^{-1})
[Fe II]	$^6D_{7/2} - ^6D_{9/2}$	384.7872	25.98839	550	2.13×10^{-3}
[S I]	$^3P_1 - ^3P_2$	396.0587	25.24878	570	1.40×10^{-3}

Note. Einstein A-values for [Fe II] 25.99 μm and [S I] 25.25 μm are from Bautista et al. (2015) and Froese Fischer et al. (2006), respectively. The wavelengths are taken from the energy levels of Nave & Johansson (2013) and Blondel et al. (2006), respectively.

The EXES observations and line profile measurements are presented and discussed in Sections 2 and 3, respectively. The results are analyzed and the implications for potential changes of [O I] 63.19 μm are given in Section 4, and the conclusions are given in Section 5.

2. SOFIA-EXES Observations

EXES provides spectral resolutions up to $R = 50{,}000–100{,}000$ and features a 1024×1024 Si:As detector array that covers 4.5–28.3 microns (Richter et al. 2018). It is a PI-class instrument that is flown on board SOFIA (Young et al. 2012). In observing Cycle 7, during the period when Betelgeuse reached its V-band brightness minimum, EXES was mounted on SOFIA and observations of the circumstellar [Fe II] 25.99 μm and [S I] 25.25 μm emission lines were obtained with the same spectrograph settings as previous observations made in Cycle 5. The [Fe II] 25.99 μm had first been observed with a different setting in Cycle 2 (Harper et al. 2017b). The times of the observations are given in Table 2, along with the V magnitudes interpolated from the light curve shown in Figure 1. The Cycle 2 and 5 observations were obtained when Betelgeuse was in its normal bright quasi-period state, while the Cycle 7 observation was taken at its minimum.

Two slits were used for the observations which were nodded along the 28″5 long apertures. The default slit width is 3″23, with a resolution of $R \simeq 65{,}000$, and a narrow 0″81 slit that provides $R \simeq 85{,}000$. For Cycles 5 and 7 the [Fe II] 25.99 μm was observed through the narrow slit, while the [S I] 25.25 μm and Cycle 2 [Fe II] 25.99 μm were observed through the default slit. At these wavelengths and high spectral-resolution there are gaps between the orders. In Cycle 5 the telluric calibrator Metis was also observed to provide the shape of the individual order sensitivities. A measure of the image quality for SOFIA that includes telescope diffraction and pointing jitter is ∼4″ FWHM; i.e., it is wider than the slit widths but smaller than the nod distance. The wavelength scales were derived from emission line obtained in adjacent orders, and for Cycle 5 and 7 the uncertainty is expected to be ≃0.5km s^{-1}. Hereafter, we refer to Cycles 2, 5, and 7 as CY02, CY05, and CY07.

3. Results

The spectral orders for the [Fe II] 25.99 μm setting are shown in Figure 2. In Cycle 7 the order shapes appear relatively flat, while for Cycle 5 we have used the telluric calibrator Metis to apply a polynomial correction to the continuum shape. There are noticeable differences in the shape of the in-order continua, especially the small-scale features present in Cycle 7 that have characteristic scales of ∼15 km s^{-1}. To compare the observed continua with theoretical models we have computed synthetic spectra from a grid

Table 2
SOFIA-EXES Observations of Betelgeuse

Program ID	[Fe II]	[S I]	V Magnitude
	UT yr-mon-day hh:min		
Cycle 2 02_004	2015 Mar 3 15:19	⋯	0.46
Cycle 5 05_007	2017 Mar 22 06:16	2017 Mar 22 06:50	0.31
Cycle 7 75_005	2020 Feb 15 04:51	2020 Feb 15 05:09	1.59

Note. UT time of mid-observation.

of spherical MARCS photospheric models (Gustafsson et al. 2008). The models have $T_{eff} = 3600, 3500, 3400, 3300, 3200$ K, $\text{Log}(g_*) = 0.0$, solar abundances, except for a lower C^{12}/C^{13} ratio typical of red giants. The synthetic spectra have been convolved with a $v_{macro} = 15$km s^{-1}. For this spectral region, there is perhaps some correspondence of the absorption features in CY07; however, the MARCS models are not a good match at any of the epochs. The star's continuum at 25.99 μm has contributions from the photosphere and optically thin olivine silicate dust emission that dominates at $\lambda > 17\,\mu$m (Verhoelst et al. 2006). It is also likely that the continuum has a component from the molecular reservoir located between the photosphere and chromosphere (Tsuji 2006; Perrin et al. 2007; Montargès et al. 2014). Under these circumstances it is reasonable to expect that there will be some mismatch between the observed and MARCS synthetic spectra.

The CY02, CY05, and CY07 [Fe II] 25.99 μm emission line profiles are shown in Figure 3 where we have normalized the continuum at 384.75 cm^{-1} to 1100 Jy, based on the IRAS 25 μm PSC flux (Beichman et al. 1988), color-corrected with the ISO-SWS spectrum (Justtanont et al. 1999; Sloan et al. 2003). It is remarkable how similar the line to continuum flux ratios are for these epochs.

To compare the [Fe II] 25.99 μm line properties, a Voigt profile and low-order polynomial were used to model the strong telluric feature near 384.90 cm^{-1}. We fit simple Gaussian profiles to the emission lines that provide a very good fit, although there is a small excess in the wings. Shown in this way the differential properties are more clearly seen. The integrated [Fe II] 25.99 μm flux to the local continuum flux ratios for CY02:CY05:CY07 are 0.85:1.00:1.04. The CY05 and CY07 ratios are very similar to each other and were observed with the same settings, while the CY02 observation used a wider slit that would lead to slightly more CSE silicate dust continuum emission passing through the aperture and potentially reducing the ratio. For the centroid velocities we adopt a center-of-mass (C-o-M) radial velocity of Betelgeuse of $V_{rad} = 20.9 \pm 0.3$ (Harper et al. 2017b), which is in good agreement with the more recent value of $V_{rad} = 20.7 \pm 0.2$ km s^{-1} derived from modeling of spatially resolved stellar rotation in SiO and CO spectra measured with Atacama Large
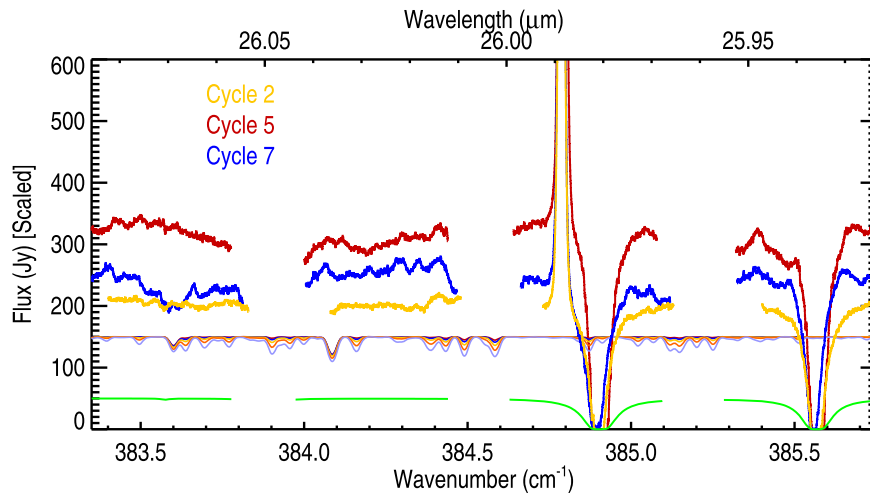
Figure 2. Spectral orders near the [Fe II] 25.99 μm line. The bottom green line is the sky spectrum, which shows the two strong telluric features. The spherical MARCS model synthetic photospheric spectra are shown below the observed spectra, normalized to 150 Jy, show the change in depth of photospheric absorption features as the effective temperature declines. The curves are, from the top downward, for T_{eff} = 3600, 3500, 3400, 3300, 3200 K.
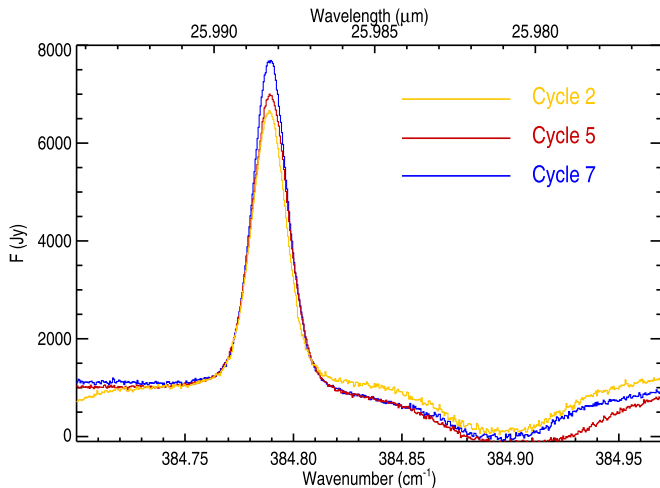
Figure 3. Cycle 2, 5, and 7 [Fe II] 25.99 μm profiles, with CY05 and CY07 obtained with the same spectrograph setup. The profiles are centered on the stellar rest frame, except an additional shift of 2.6 km s^{-1}, has been applied to CY07. The continua have been normalized at 384.75 cm^{-1}, close to the emission line. Note the very close agreement between the line and continuum in Cy05 and Cy07. Note that the emission lines sit upon the far wing of the very strong telluric feature at 384.90 cm^{-1}.

Table 3
EXES Line Profile Measurements

Observation Date	[Fe II]		[S I]	
	V_{cent}	V_{FWHM}	V_{cent}	V_{FWHM}
2015 Mar 3	-1.9 ± 0.4	15.0 ± 0.3	$\cdots$	$\cdots$
2017 Mar 22	-0.3 ± 0.5	15.8 ± 0.3	-1.7 ± 0.5	13.4 ± 0.4
2020 Feb 15	$+1.3 \pm 0.5$	15.0 ± 0.3	-1.5 ± 0.5	13.8 ± 0.4

Note. All velocity measurements in km s^{-1}.

Millimeter/submillimeter Array (ALMA) by Kervella et al. (2018). Observations of the photospheric radial velocity have been made during the V-band dimming and the velocity of the photosphere has increased by 10 km s^{-1} moving from blue-shifted to redshifted (T. Granzer & K. Strassmeier 2020, private communication). At the time of the EXES CY07 observation $V_{phot} \simeq +2.6$ km s^{-1} in the C-o-M frame.

The line profile measurements of the [Fe II] 25.99 μm are given in Table 3. The velocity centroids and line widths measured in this similar manner show no major changes.[7] The uncertainties given here are based on the line fits and changes resulting from different continuum shape models. The difference in velocity centroids between CY05 and CY07 may be real because the observations used the same spectral settings and wavelength calibration. This could indicate a slight

reduction in outflow velocity in the line-forming region; however, differences in the strong telluric feature and stellar continuum shape must be considered.

The spectral orders near the [S I] 25.25 μm are shown in Figure 4, and here there is a good correspondence between the continuum features in CY05 and CY07. Again, there is not a good agreement with the MARCS simulations. In CY07 the pair of strong water features near 394.9 cm^{-1} have deepened. Given that the continuum has a contribution from silicate dust emission the features are much deeper than predicted by the coolest MARCS model, with $T_{eff} = 3200$ K.

The two [S I] 25.25 μm emission profiles are shown in Figure 5 and it can be seen that these lines do not show a significant change in flux to continuum ratio either. An examination of the [S I] 25.25 μm spectral region of α Sco (M1.5 Iab) obtained in Cycle 5, which shows no emission line, presumably a result of photoionization by the binary companion, shows a similar continuum to CY05. The [S I] 25.25 μm line measurements are given in Table 3. Again, the dynamical properties are very similar between CY05 and CY07. Note that the wavelength of the [Fe II] 25.99 μm line is quite accurately known, while the [S I] 25.25 μm line wavelength has an intrinsic uncertainty of 1σ $(v) = 2.4$ km s^{-1} (Blondel et al. 2006), so the value of the centroid velocities have a significant additional systematic uncertainty.

The [Fe II] 25.99 μm and [S I] 25.25 μm spectra reveal that the emission line properties have changed very little between the epochs, especially when the uncertainties in the profile measurements and the uncertain intrinsic continua are considered. It would seem contrived that the emission line and

---

[7] The line width of CY02 is slightly larger than reported previously because of the different telluric correction model.
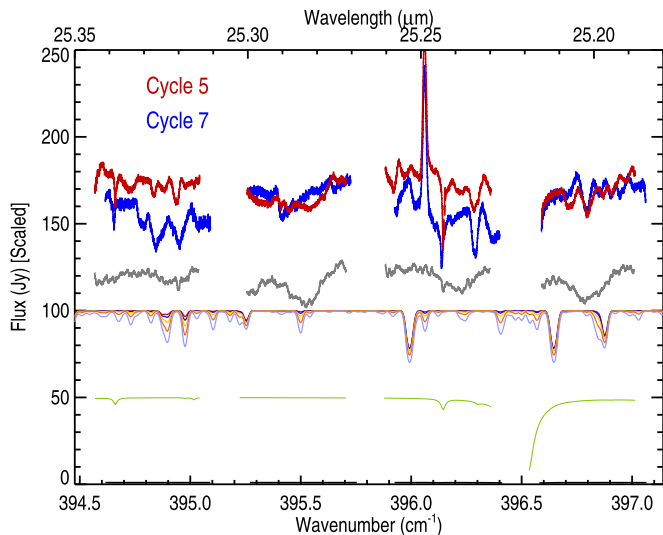
Figure 4. Spectral orders near the [S I] 25.25 μm line. The CY05 (red) and CY07 (blue) are uncorrected for order shape, and the CY05 Metis spectrum is shown in gray highlighting how the order shape can affect the stellar spectra. The most significant difference between CY05 and CY07 are the deepening of the strong water absorption lines in CY07 near 394.9 cm^{-1}. The bottom green line shows the sky spectrum. The spherical MARCS model spectra, normalized to 100 Jy, are described in Figure 2. Again, there is not a strong correspondence between the photospheric models and the observed structure, in particular the feature on the high-frequency side of the [S I] 25.25 μm emission.
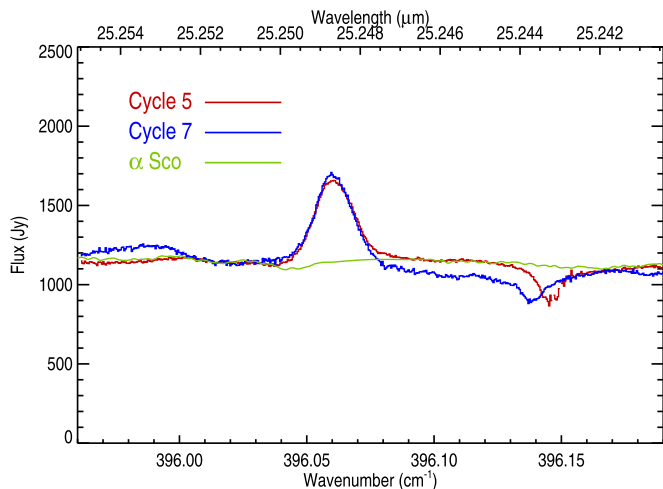
Figure 5. Betelgeuse Cycle 5 and 7 [S I] 25.25 μm profiles obtained with the identical spectrograph setup. The radial velocity Doppler shifts have been applied. Arbitrarily, the continua have been normalized at 396.30 cm^{-1}. A previous observation of α Sco (M1.5 Iab) shows no [S I] 25.25 μm emission, but its continuum near the emission line follows that of Betelgeuse in Cycle 5. α Sco's smoothed, and corrected for a telluric feature near 25.25 μm, is shown in green. Like the [Fe II] 25.99 μm lines, the [S I] 25.25 μm lines show very similar line widths, centroid velocities, and similar flux to continuum ratios. Apart from changes in the continuum structure the circumstellar emission in the two lines at both epochs are very similar, suggesting that the photospheric changes have not affected the region between 2 an 25R_* (see the Discussion). Note the telluric features near 396.14 cm^{-1}.

continuum fluxes would change in concert at different epochs, and with the similar line widths and velocity centroids it is reasonable to conclude that the CSE gas emitting these lines has not responded in a significant way to the changes that led to the 2020 February V-band minimum. The CSE is not responding to either changes in the photosphere and/or to the potential presence of new dust in the sightline to the star.

3.1. [Fe II] 25.99 μm to [S I] 25.25 μm Flux Ratios

We can also examine the [Fe II] 25.99 μm to [S I] 25.25 μm flux ratios for the 2017 and 2020 epochs by noting that the continuum flux ratio for 25.25–25.99 μm is expected to be close to unity, i.e., $\simeq 1.07$, based on the shape of the ISO-SWS spectra (Justtanont et al. 1999; Sloan et al. 2003). This gives a [Fe II] to [S I] integrated line flux ratio of ~ 15, which we can compare to theoretical predictions.

Carr et al. (2000) reported a near-solar iron abundance for Betelgeuse [Fe/H] $= -0.02 \pm 0.08$ (with $A(S)_\odot = 1.32 \times 10^{-5}$ and $A(Fe)_\odot = 3.16 \times 10^{-5}$ (Asplund et al. 2009)). Both transitions are between the two lowest ground term fine-structure levels, and have similar Einstein A-values (see Table 1). Neutral iron has a low first ionization potential (7.90 eV) and is easily photoionized by the stellar ultraviolet continuum with $\lambda < 1570$ Å, while the second ionization potential is high (16.20 eV) resulting in Fe II being the dominant ionization state of the gas phase of the chromosphere and CSE outflow. Neutral sulfur has a high first ionization potential of 10.36 eV with a ground state photo-ionization edge at 1195 Å and requires far-ultraviolet flux to become photoionized. Sulfur is also expected to have a low association in any dust associated with the wind (Snow et al. 1987).

Both electron and neutral hydrogen collisions can drive a Boltzmann distribution for the low-lying fine-structure levels. While the electron density, n_e, is expected to be much lower than for hydrogen, n_H, it has larger collisional de-excitation rates. Electron collision rates are available for S I from Tayal (2004) and Fe II from Bautista et al. (2015, and 2020, private communication), S+H collision rates can be estimated using the O+H rates of Lique et al. (2018), and Fe+H rates are given by Hollenbach & McKee (1989). Using the thermodynamic models of Rodgers & Glassgold (1991), Harper et al. (2001), or Harper et al. (2017b; where the gas temperatures are reduced close to the star) both lines are formed predominantly above the critical densities (i.e., thermalized) when $T_{gas} > 500$ K. If Fe II and S I and are dominant ionization states, then the ratio of [Fe II] 25.99 μm and [S I] 25.25 μm fluxes, would be $\leqslant 4.5$ in the optically thin limit, and lower, ~ 1.5, when allowing for optical depth effects. The observations suggest then that the CSE sulfur is partially photoionized to S II by the stellar chromosphere, where H I Lyβ is the strongest source of line photons. The similarity of the flux ratios between 2017 and 2020 also suggest that there has not been a strong change in the far-ultraviolet radiation field, although if H I Lyβ is a major photoionizing source then there will be a time-lag for the photons in this very opaque line to escape to the CSE.

4. Discussion

The EXES observations show no significant changes in the velocity centroids and line widths between 2015 and 2017, and 2020 February when the V-band brightness reached its minimum state. The line-to-continuum ratios also show no evidence that the wind heating has changed. The event leading to the great dimming in V-band has not significantly affected the inner circumstellar outflow. Magnetic fields have long been considered a candidate for driving the outflows from RSG (Hartmann & Avrett 1984), and Betelgeuse's measured magnetic field (Aurière et al. 2010) appears typical of other RSGs (Tessore et al. 2017). The timescale for photospheric

magnetic field variations (Mathias et al. 2018) is consistent with the 5.8 yr timescale observed in radial velocity and V magnitudes, which has been attributed to giant convective cells. If this is the case, the large-scale morphology of the open magnetic field lines might be modified by the emergence of a new large cool convective cell, one might expect that the Alfvén wave properties and wind acceleration might respond to such a change.

The thermodynamic models of Harper et al. (2017b) suggest that the [Fe II] 25.99 μm and [S I] 25.25 μm lines are predominantly formed within 3–$20R_*$. Assuming a distance of 222 pc (Harper et al. 2017a), this corresponds to a light-crossing time of a few hours. The radius of the peak mean chromospheric temperature derived from radio continuum observations is $\simeq 1.75\,R_*$ (O'Gorman et al. 2015), and if the atmospheric disruption has disturbed the magnetic field in this region then the time for outward-propagating Alfvén waves to cross this region can be estimated. Using the thermodynamic model of Harper et al. (2001), and assuming a radial magnetic field with $B(1.75R_*) \sim 5$ G, a typical value expected on energetic grounds (e.g., Hartmann & Avrett 1984), the Alfvén wave-crossing time to $10R_*$ is of the order of a decade. The absence of changes in the CSE emission in this region is consistent with photospheric changes in large-scale magnetic fields that have not yet reached the inner CSE.

The pattern of V magnitude and [O I] fluxes noted by Haas et al. (1995), if confirmed, might then result from a change in wind heating caused by gas-dust grain collisions in a region where $T_{\rm gas} < 500$ K. Haas et al. (1995) suggested that the [O I] 63.19 μm fluxes might be related to V-band brightness changes through a change in the dust grain drift velocity (Goldreich & Scoville 1976). The [O I] 63.19 μm has flux contributions that overlap the [Fe II] 25.99 μm and [S I] 25.25 μm lines but also extends farther out to $\sim 3''$ ($\sim 130R_*$).

The theoretical study of the CSE's thermal steady-state structure by Rodgers & Glassgold (1991) showed that the onset of CSE dust heating, near $30R_*$ is matched by a peak in [O I] 63.19 μm cooling. Dust can respond quickly to changes in the photospheric illumination, and the dust-gas heating rate per unit volume H is proportional to the cube of the dust-drift velocity, or to changes in effective luminosity in the *steady state* as $H \propto L^{3/2}$. However, there also will be a temporal lag between changes in the luminosity and heating of the gas. While the V magnitude has increased by $\Delta V \simeq 1$ mag since 2009 September, the narrow-band Wing 1.0240 μm C-band photometry reveals a smaller increase of $\Delta C \simeq 0.3$ mag, so it is not clear what the magnitude of the changes in dust properties are likely to be. However, assuming a radiation pressure efficiency of $Q_{\rm Pr} = 0.05$, a grain radius of 0.1 μm, and gas densities from CSE models, the periodic dust-drift velocity lags the luminosity variations by ~ 20 days. The collisional excitation and radiative decay timescales for the [O I] 63.19 μm are about a week so it is possible that, in regions where dust heating dominates the CSE energy balance, changes in stellar luminosity can modify the gas temperature on timescales much shorter than Betelgeuse's 420 day period.

Reducing the dust heating in the CSE gas will only reduce the emission lines fluxes if its magnitude is comparable to other heating and cooling processes. For the [Fe II] 25.99 μm and [S I] 25.25 μm lines, the dust plumes seen at similar formation radii in images, may be such an example, or instead the dust may represent a small volume filling factor.

5. Conclusions

These EXES results, which do not reveal significant changes in the [Fe II] 25.99 μm and [S I] 25.25 μm emission lines between 2017 March and 2020 February, when combined with contemporaneous and future multi-wavelength observations will help to clarify the nature of the 2019–2020 V-band dimming of Betelgeuse and its subsequent effect on the extended atmosphere. The EXES results suggest that dust in the inner CSE is not significantly heating the gas. At the time of submission of this Letter SOFIA will be observing Betelgeuse with the Far Infrared Field-Imaging Line Spectrometer (FIFI-LS; Fischer et al. 2018; Colditz et al. 2018), upGREAT (Risacher et al. 2018).

ORCID iDs

Graham M. Harper ● https://orcid.org/0000-0002-7042-4541
Curtis N. DeWitt ● https://orcid.org/0000-0002-6528-3836
Matthew J. Richter ● https://orcid.org/0000-0002-8594-2122
Edward F. Guinan ● https://orcid.org/0000-0002-4263-2650
Nils Ryde ● https://orcid.org/0000-0001-6294-3790
Amanda J. Townsend ● https://orcid.org/0000-0002-6377-4869

References

Asplund, M., Grevesse, N., Sauval, A. J., & Scott, P. 2009, ARA&A, 47, 481
Aurière, M., Donati, J.-F., Konstantinova-Antova, R., et al. 2010, A&A, 516, L2
Bautista, M. A., Fivet, V., Ballance, C., et al. 2015, ApJ, 808, 174
Beichman, C. A., Neugebauer, G., Habing, H. J., Clegg, P. E., & Chester, T. J. 1988, Infrared Astronomical Satellite (IRAS) Catalogs and Atlases.Volume 1: Explanatory Supplement (Washington, DC: NASA)
Blondel, C., Chaibi, W., Delsart, C., & Drag, C. 2006, JPhB, 39, 1409
Carr, J. S., Sellgren, K., & Balachandran, S. C. 2000, ApJ, 530, 307
Castro-Carrizo, A., Bujarrabal, V., Fong, D., et al. 2001, A&A, 367, 674
Colditz, S., Beckmann, S., Bryant, A., et al. 2018, JAI, 7, 1840004
Dolan, M. M., Mathews, G. J., Lam, D. D., et al. 2016, ApJ, 819, 7
Dupree, A. K., Baliunas, S. L., Guinan, E. F., et al. 1987, ApJL, 317, L85
Fischer, C., Beckmann, S., Bryant, A., et al. 2018, JAI, 7, 1840003
Froese Fischer, C., Tachiev, G., & Irimia, A. 2006, ADNDT, 92, 607
Goldberg, L. 1984, PASP, 96, 366
Goldreich, P., & Scoville, N. 1976, ApJ, 205, 144
Guinan, E., Deeney, B., & Miller, K. 1993, IAUC, 5708, 1
Guinan, E., Wasatonic, R., Calderwood, T., & Carona, D. 2020, ATel, 13512, 1
Guinan, E. F., & Wasatonic, R. J. 2020, ATel, 13439, 1
Gustafsson, B., Edvardsson, B., Eriksson, K., et al. 2008, A&A, 486, 951
Haas, M. R., & Glassgold, A. E. 1993, ApJL, 410, L111
Haas, M. R., Glassgold, A. E., & Tielens, A. G. G. M. 1995, in ASP Conf. Ser. 73, From Gas to Stars to Dust, ed. M. R. Haas, J. A. Davidson, & E. F. Erickson (San Francisco, CA: ASP)
Harper, G. M., Brown, A., & Guinan, E. F. 2008, AJ, 135, 1430
Harper, G. M., Brown, A., Guinan, E. F., et al. 2017a, AJ, 154, 11
Harper, G. M., Brown, A., & Lim, J. 2001, ApJ, 551, 1073

Harper, G. M., DeWitt, C., Richter, M. J., et al. 2017b, ApJ, 836, 22
Harper, G. M., Richter, M. J., Ryde, N., et al. 2009, ApJ, 701, 1464
Hartmann, L., & Avrett, E. H. 1984, ApJ, 284, 238
Hollenbach, D., & McKee, C. F. 1989, ApJ, 342, 306
Justtanont, K., Tielens, A. G. G. M., de Jong, T., et al. 1999, A&A, 345, 605
Keenan, P. C., & McNeil, R. C. 1989, ApJS, 71, 245
Kervella, P., Decin, L., Richards, A. M. S., et al. 2018, A&A, 609, A67
Kervella, P., Lagadec, E., Montargès, M., et al. 2016, A&A, 585, A28
Kervella, P., Le Bertre, T., & Perrin, G. 2013, EAS Publications Ser. 60,
    Betelgeuse Workshop 2012 (Les Ulis: EDP Sciences)
Kervella, P., Perrin, G., Chiavassa, A., et al. 2011, A&A, 531, A117
Kervella, P., Verhoelst, T., Ridgway, S. T., et al. 2009, A&A, 504, 115
Kiss, L. L., Szabó, G. M., & Bedding, T. R. 2006, MNRAS, 372, 1721
Krisciunas, K. 1992, IBVS, 3728, 1
Krisciunas, K. 1994, IBVS, 4028, 1
Levesque, E. M., & Massey, P. 2020, ApJL, 891, L37
Lique, F., Kłos, J., Alexander, M. H., Le Picard, S. D., & Dagdigian, P. J.
    2018, MNRAS, 474, 2313
Lobel, A., & Dupree, A. K. 2001, ApJ, 558, 815
Mathias, P., Aurière, M., López Ariste, A., et al. 2018, A&A, 615, A116
Meynet, G., Chomienne, V., Ekström, S., et al. 2015, A&A, 575, A60
Montargès, M., Kervella, P., Perrin, G., et al. 2014, A&A, 572, A17
Nave, G., & Johansson, S. 2013, ApJS, 204, 1
O'Gorman, E., Harper, G. M., Brown, A., et al. 2015, A&A, 580, A101

O'Gorman, E., Harper, G. M., Brown, J. M., et al. 2012, AJ, 144, 36
Perrin, G., Verhoelst, T., Ridgway, S. T., et al. 2007, A&A, 474, 599
Richter, M. J., Dewitt, C. N., McKelvey, M., et al. 2018, JAI, 7, 1840013
Risacher, C., Güsten, R., Stutzki, J., et al. 2018, JAI, 7, 1840014
Rodgers, B., & Glassgold, A. E. 1991, ApJ, 382, 606
Sanford, R. F. 1933, ApJ, 77, 110
Skinner, C. J., Dougherty, S. M., Meixner, M., et al. 1997, MNRAS, 288, 295
Sloan, G. C., Kraemer, K. E., Price, S. D., & Shipman, R. F. 2003, ApJS,
    147, 379
Smartt, S. J. 2009, ARA&A, 47, 63
Smith, M. A., Patten, B. M., & Goldberg, L. 1989, AJ, 98, 2233
Smith, N., Hinkle, K. H., & Ryde, N. 2009, AJ, 137, 3558
Snow, Theodore P., Buss, J., Richard, H., Gilra, D. P. J., & Swings, J. P. 1987,
    ApJ, 321, 921
Spencer Jones, H. 1928, MNRAS, 88, 660
Stebbins, J. 1931, PWasO, 15, 177
Sukhbold, T., & Adams, S. 2020, MNRAS, 492, 2578
Tayal, S. S. 2004, ApJS, 153, 581
Tessore, B., Lèbre, A., Morin, J., et al. 2017, A&A, 603, A129
Tsuji, T. 2006, ApJ, 645, 1448
Verhoelst, T., Decin, L., van Malderen, R., et al. 2006, A&A, 447, 311
Weymann, R. 1962, ApJ, 136, 844
White, N. M., & Wing, R. F. 1978, ApJ, 222, 209
Young, E. T., Becklin, E. E., Marcum, P. M., et al. 2012, ApJL, 749, L17